Kobe University Repository : Kernel

PDF issue: 2025-07-20

Semi-empirical correlation for counter-current flow limitation at the upper or lower end of sharp-edged vertical pipes

Goda, Raito
Hayashi, Kosuke
Kirkland, Karen Vierow
Murase, Michio
Tomiyama, Akio

(Citation)
Nuclear Engineering and Design,328:182-187

(Issue Date)
2018-03

(Resource Type)
journal article

(Version)
Accepted Manuscript

(Rights)
© 2018 Elsevier B.V.
This manuscript version is made available under the CC-BY-NC-ND 4.0 license
http://creativecommons.org/licenses/by-nc-nd/4.0/

(URL)
https://hdl.handle.net/20.500.14094/90004932

KOBE UNIVERSITY

Semi-empirical correlation for counter-current flow limitation at the upper or lower end of sharp-edged vertical pipes

Raito Goda[a], Kosuke Hayashi[a], Karen Vierow Kirkland[b], Michio Murase[c], Akio Tomiyama[a,*]

[a] *Graduate School of Engineering, Kobe University, 1-1 Rokkodai Nada Kobe Hyogo, 657-8501 Japan*
[b] *Texas A&M University, 400 Bizzell St, College Station, TX 77843 USA*
[c] *Institute of Nuclear Safety System, 64 Sata Mihama-cho Mikata-gun Fukui, 919-1205 Japan*

Abstract

A semi-empirical correlation for CCFL (counter-current flow limitation) in vertical pipes was derived from one-dimensional momentum equations. Available correlations such as the empirical correlations proposed by Wallis (1969) and Zapke and Kröger (1996) can be deduced from the derived fundamental functional form of the semi-empirical correlation in limiting flow conditions. Comparisons between the semi-empirical correlation with available experimental data of CCFL taking place at the sharp-edged lower end of a vertical pipe showed that the correlation is applicable for various fluid properties and pipe diameters. The fundamental functional form of the correlation was also transformed so as to express the characteristics of CCFL occurring at the sharp-edged upper end of a vertical pipe. The present fundamental functional form of CCFL correlation is useful not only to express CCFL data but also to understand how relevant parameters play their roles in the CCFL characteristics.

Keywords: counter-current flow, vertical pipe, CCFL correlation, flooding

*Corresponding author
Email address: tomiyama@mech.kobe-u.ac.jp (Akio Tomiyama)

1. Introduction

A falling liquid film in a vertical pipe and a gas core flowing upward form a two-phase counter-current annular flow. The liquid supplied into the pipe can entirely fall down when the gas volume flux is small. While keeping the liquid inflow constant, the increase in the gas volume flux results in wavy structure on the gas-liquid interface. Some liquid then begins to flow back toward the liquid-inlet side at a certain gas volume flux due to the fast upward motion of the gas (counter-current flow limitation, CCFL). The liquid and gas volume fluxes at the onset of the upward motion of the liquid phase is referred to as the flooding point and the flooding points form the so-called flooding curve. Further increase in the gas volume flux decreases the flow rate of the falling liquid. The relationship between the gas volume flux and the actual liquid flow rate under CCFL is referred to as the CCFL characteristics.

The practical importance of knowledge on the counter-current two-phase flow, especially in nuclear and chemical engineering, has resulted in a large number of studies on the counter-current two-phase flows in vertical pipes (Wallis, 1969; Wallis and Makkenchery, 1974; Richter, 1981; Bharathan and Wallis, 1983; Govan et al., 1991; Bankoff and Lee, 1986; Jeong and No, 1996; Zapke and Kröger, 1996, 2000a,b; Karimi and Kawaji, 2000; Vijayan et al., 2001; Schmidt et al., 2016) (it should be noted that, in the literature, the onset of flooding and the CCFL characteristics were not clearly distinguished and the location of the flow limitation was rarely reported, and therefore, we should be careful when using the available data). For example, CCFL may take place in the steam generator of a pressurized water reactor (PWR) during a reflux-cooling mode, and therefore, CCFL correlations are required to evaluate the flow rate of liquid flowing into the reactor core. Hence we have been investigating the CCFL characteristics in vertical pipes (Kusunoki et al., 2015, 2016; Murase et al., 2016) and proposed some CCFL correlations (Kusunoki et al., 2015), which account for the effects of the fluid properties on the CCFL characteristics. The correlations were however obtained by a purely empirical manner.

In this study, a semi-empirical correlation for CCFL characteristics in vertical pipes is derived from one-dimensional equations for a counter-current annular two-phase flow in a vertical pipe, and its applicability to several data of CCFL characteristics is discussed.

2. Brief review of CCFL correlations

Wallis (1969) proposed the following CCFL correlation based on several experimental data:

$$J_G^{*1/2} + m J_L^{*1/2} = C \tag{1}$$

where m and C are the slope and the intercept of the $J_L^{*1/2}$-$J_G^{*1/2}$ diagram, the subscripts G and L denote the gas and liquid phases, respectively, and J_k^* are

the Froude numbers or the so-called Wallis parameters defined by

$$J_k^* = \frac{J_k}{\sqrt{\frac{\Delta\rho g D}{\rho_k}}} \tag{2}$$

Here J is the volume flux, ρ the density, g the magnitude of the acceleration of gravity, D the pipe diameter, and $\Delta\rho$ the density difference, i.e. $\Delta\rho = \rho_L - \rho_G$, between the liquid and gas phases. This correlation has been widely used in correlating CCFL data in vertical pipes. The m and C depend on the inlet and outlet geometries of a vertical pipe and on the inverse viscosity number, N_L, of the liquid phase defined by

$$N_L = \sqrt{\frac{\rho_L \Delta\rho g D^3}{\mu_L^2}} \tag{3}$$

where μ is the viscosity. Equation (1) represents the balance between the inertial forces of the gas and liquid phases and the gravitational force. The effects of the liquid viscosity and the surface tension are not accounted for. Wallis (1969) took into account the effects of the liquid viscosity on CCFL by introducing N_L by an empirical manner:

$$J_G^{*1/2} + 5.6\left(\frac{J_L^*}{N_L}\right)^{1/2} = 0.725 \tag{4}$$

He also pointed out that this expression is valid for $N_L < 2$ and the slope and the intercept should be functions of N_L for larger N_L.

Wallis (1969) derived the functional form of Eq. (1) by using an annular flow model (Fig. 1), in which the gas and liquid phases are modeled as the cylindrical gas core and the liquid annulus. By assuming that the flows of the two phases are turbulent and the mixing lengths in each phase are constant, the momentum equations of the two phases reduce to

$$\frac{J_G^{*1/2}}{\alpha_G^n} + \frac{J_L^{*1/2}}{\alpha_L^n} = 1 \tag{5}$$

where α is the volume fraction and $\alpha_G + \alpha_L = 1$. The n is 2.5 if the mixing lengths are scaled by the characteristic length scales of each phase, or $n = 3.5$ if they are scaled by D. Eliminating α_k from this equation yields the following envelope:

$$J_G^{*2/(n+1)} + J_L^{*2/(n+1)} = 1 \tag{6}$$

If $n = 3$, this equation reduces to Eq. (1) with $m = C = 1$. Bharathan and Wallis (1983) derived the following relation between $J_G^{*1/2}$ and $J_L^{*1/2}$ in terms of α_L and the interfacial friction, f_i, and the wall friction factors, f_W:

$$\left[\frac{2f_i}{(1-\alpha_L)^{5/2}}\right] J_G^{*2} + \left[\frac{2f_W}{\alpha_L^2}\right] J_L^{*2} = \alpha_L \tag{7}$$

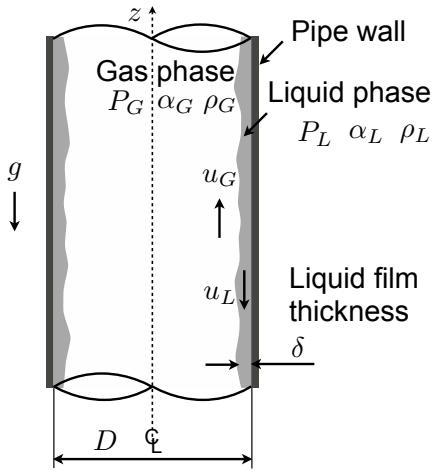

Figure 1: Annular flow model for counter-current two-phase flow

The friction factors were given empirically. Since the above equation does not have a simple solution for the Wallis parameters, the envelope was graphically obtained by changing α_L as the parameter. The annular flow model was also applied to the viscous-force-dominant case, Eq. (4) (Wallis, 1969). In this case, the momentum balance reduces to

$$\left(\frac{J_G^{*2}}{\Delta P^*}\right)^{1/n} + \left[\frac{32 J_L^*}{N_L(1-\Delta P^*)}\right]^{1/2} = 1 \tag{8}$$

where ΔP^* is the pressure drop scaled by the buoyancy. The envelope can be obtained parametrically in terms of ΔP^*.

Kusunoki et al. (2015) experimentally investigated the effects of the liquid viscosity on flow limitation at the sharp-edged lower end of a vertical pipe (CCFL-L). In this mode of flow limitation, the liquid flow is limited at the lower end of the pipe and some amount of liquid accumulated there is intermittently brought up by the gas flow (Govan et al., 1991; Kusunoki et al., 2015). The following empirical correlation was proposed to take into account the effects of the gas and liquid viscosities on CCFL-L:

$$\left(\frac{\mu_G}{\mu_L}\right)^{-0.07} J_G^{*1/2} = (1.04 \pm 0.05) - 3.6\Psi + 11\Psi^2 - 16\Psi^3 \tag{9}$$

where

$$\Psi = \left(\frac{\mu_G}{\mu_L}\right)^{0.1} J_L^{*1/2} \tag{10}$$

Zapke and Kröger (1996) investigated the effects of the liquid viscosity and the surface tension σ on CCFL. They showed that their data for various fluid

properties can be well correlated by introducing the Ohnesorge number, Oh_L, of the liquid phase into the Wallis-type empirical correlation, i.e.

$$J_G^{*1/2} + J_L^{*1/2} = 0.52 Oh_L^{-0.05} \tag{11}$$

where

$$Oh_L = \sqrt{\frac{\mu_L^2}{\rho_L \sigma D}} \tag{12}$$

The counter-current flow limitation at the sharp-edged upper end of a vertical pipe (CCFL-U) was also investigated in our previous study (Doi et al., 2012). Under CCFL-U, the sharp-edged upper end of the pipe is connected to an upper tank filled with the liquid, and then, the gas blows out to the upper tank as large bubbles, which causes the liquid penetration into the pipe. Thus the bubble generation process plays an important role in the liquid flow rate. The characteristics of CCFL-U is more complicated than CCFL-L since it depends on the tank geometry, the liquid level, h_T, in the upper tank and the gas volume, V_T, in the lower tank. In spite of the complex nature of CCFL-U, the experiments confirmed that the CCFL characteristics are independent of h_T at small V_T and large h_T or are independent of V_T when h_T is small. Doi et al. (2012) also confirmed that the pipe diameter has negligible effects on the CCFL characteristics, and therefore, the following Kutateladze parameter is more appropriate than the Wallis parameters for correlating CCFL-U:

$$Ku_k = \frac{J_k}{\left[\frac{\Delta\rho g \sigma}{\rho_k^2}\right]^{1/4}} \tag{13}$$

The Kutateladze parameter has been recommended for large diameter pipes, and Wallis and Makkenchery (1974) proposed the criterion, $D^* \ (= D/[\sigma/\Delta\rho g]^{1/2}) > 30$, for which the Kutateladze-type correlation is appropriate (Wynne et al., 2016). This criterion was however obtained for a round-edged upper end, whereas the upper end in the CCFL experiments in our previous study (Doi et al., 2012) was sharp-edged (Kusunoki et al., 2017). In the latter, the flow limitation at the upper end was confirmed even at $D^* = 11$. This fact implies that the geometry of the end of the pipe affects the critical D^*. Murase et al. (2016) fitted the CCFL data of Doi et al. (2012) and Richter (1981) using Ku_k and obtained the following empirical correlation:

$$Ku_G^{1/2} + 0.90 Ku_L^{1/2} = 1.5 \pm 0.1 \tag{14}$$

The models, Eqs. (7) and (8), accounting for the fluid properties were given in the parametric forms, and therefore, ΔP^* (or α_G) must be specified to obtain the J_L^*-J_G^* diagram. Although Eqs. (9) and (11) account for the effects of the fluid properties, these correlations were derived in purely empirical manners. In the following section, we derive a semi-empirical CCFL correlation accounting for the effects of the fluid properties. The initial stage of the derivation is similar

to that for the correlation by Bharathan and Wallis (1983), whereas the envelope in the present correlation is expressed in terms only of the Wallis parameters (or the Kutateladze parameters).

3. Fundamental functional form of CCFL correlation

3.1. Derivation

The one-dimensional momentum equations of the gas and liquid phases for the annular flow model (Fig. 1) are given by

$$\frac{\partial \rho_G \alpha_G u_G}{\partial t} + \frac{\partial \rho_G \alpha_G u_G^2}{\partial z} = -\alpha_G \frac{\partial P_G}{\partial z} - \frac{Pe_i}{S}\tau_i - \rho_G \alpha_G g \tag{15}$$

$$\frac{\partial \rho_L \alpha_L u_L}{\partial t} + \frac{\partial \rho_L \alpha_L u_L^2}{\partial z} = -\alpha_L \frac{\partial P_L}{\partial z} + \frac{Pe_i}{S}\tau_i + \frac{Pe_W}{S}\tau_W - \rho_L \alpha_L g \tag{16}$$

where t is the time, u the velocity, τ_W the wall shear stress, τ_i the interfacial shear stress, Pe_W the wetted perimeter at the pipe wall, i.e. $Pe_W = 4S/D$, and Pe_i the perimeter of the interface, which is given by $Pe_i = 4S\alpha_G^{1/2}/D$, and S the cross-sectional area of the pipe. Counter-current two-phase flows in vertical pipes are unsteady, e.g. the flow limitation in CCFL-L is characterized by intermittent formation of liquid lump rising from the lower end toward the upper pipe end. Yet CCFL characteristics have usually been investigated based on the time-averaged flow rate of liquid film flowing through the lower pipe end, not on the instantaneous flow rate. We follow this way in deriving a semi-empirical correlation, and therefore, the time derivatives in the above equations are neglected. In addition, although the liquid film could be non-uniform in the axial direction, the present modeling assumes a uniform flow with an averaged liquid film thickness (Bharathan and Wallis, 1983), by neglecting the advection terms in the momentum equations. The single-pressure assumption is also employed. Thus

$$-\alpha_G \frac{dP}{dz} - \frac{Pe_i}{S}\tau_i - \rho_G \alpha_G g = 0 \tag{17}$$

$$-\alpha_L \frac{dP}{dz} + \frac{Pe_i}{S}\tau_i + \frac{Pe_W}{S}\tau_W - \rho_L \alpha_L g = 0 \tag{18}$$

where $P = P_G = P_L$. Eliminating dP/dz from the two equations yields

$$\frac{Pe_i}{\alpha_G \alpha_L S}\tau_i + \frac{Pe_W}{\alpha_L S}\tau_W = \Delta\rho g \tag{19}$$

The wall shear stress is expressed as

$$\tau_W = \frac{f_W \rho_L}{2} u_L^2 \tag{20}$$

Rewriting this using $J_k = \alpha_k u_k$ gives

$$\tau_W = \frac{f_W \rho_L}{2} \frac{J_L^2}{\alpha_L^2} \tag{21}$$

The interfacial shear stress is often expressed as

$$\tau_i = \frac{f_i \rho_G}{2}(u_G - u_L)^2 \tag{22}$$

CCFL usually takes place when $u_G^2 >> u_L^2$, and therefore,

$$\tau_i \approx \frac{f_i \rho_G}{2} u_G^2 = \frac{f_i \rho_G}{2} \frac{J_G^2}{\alpha_G^2} \tag{23}$$

Under CCFL, the liquid film thickness is usually very small. Hence

$$Pe_i \approx Pe_W \tag{24}$$

Substituting Eqs. (21), (23) and (24) into Eq. (19) yields

$$\left[\frac{2f_i}{(1-\alpha_L)^3 \alpha_L}\right] \frac{J_G^2}{\Delta\rho g D/\rho_G} + \left[\frac{2f_W}{\alpha_L^3}\right] \frac{J_L^2}{\Delta\rho g D/\rho_L} \approx 1 \tag{25}$$

where $\alpha_G = 1 - \alpha_L$ was used. In a dimensionless form,

$$\left[\frac{2f_i}{(1-\alpha_L)^3 \alpha_L}\right] J_G^{*2} + \left[\frac{2f_W}{\alpha_L^3}\right] J_L^{*2} \approx 1 \tag{26}$$

Bharathan and Wallis (1983) used the following correlation of f_i in their analysis of flooding:

$$f_i = 0.005 + 10^{-0.56+9.07/D^*} \delta^{*(1.63+4.74/D^*)} \tag{27}$$

where δ^* and D^* are the dimensionless liquid film thickness and the dimensionless pipe diameter, respectively, defined by

$$\delta^* = \frac{\delta}{\sqrt{\frac{\sigma}{\Delta\rho g}}} \tag{28}$$

and

$$D^* = \frac{D}{\sqrt{\frac{\sigma}{\Delta\rho g}}} \tag{29}$$

Here δ is the liquid film thickness. They assumed that f_W has a constant value, i.e. $f_W = 0.005$. Abe et al. (1991) proposed a similar expression for f_i, whereas f_W was given as a function of the film Reynolds number, Re_L, i.e.

$$f_i = 0.005 + \delta^{*1.27} D^{*-0.37} \tag{30}$$

$$f_W = \frac{300}{Re_L} \tag{31}$$

where

$$Re_L = \frac{\rho_L J_L D}{\mu_L} \tag{32}$$

In both correlations of f_i, f_i increases with increasing δ, in other words with increasing α_L. In this study, the more general form of f_i is utilized to take into account both form drag and skin friction:

$$f_i = \frac{A'\alpha_L}{Re_G^{B'}} \tag{33}$$

where

$$Re_G = \frac{\rho_G J_G D}{\mu_G} \tag{34}$$

Following Abe et al. (1991), let us assume the following functional form for f_W:

$$f_W = \frac{A}{Re_L^B} \tag{35}$$

Here A, B, A' and B' are coefficients. It should be noted that typical values of B and B' would be unity for laminar flows, 1/4 for turbulent flows, and 0 when the form drag is much larger than the skin friction as in the case of very rough wall or highly agitated wavy interface.

Since $Re_k = J_k^* N_k$,

$$f_i = A'\alpha_L (J_G^* N_G)^{-B'} \tag{36}$$

and

$$f_W = A(J_L^* N_L)^{-B} \tag{37}$$

Substituting these expressions of the friction factors into Eq. (26) yields

$$\left[\frac{2A'N_G^{-B'}}{(1-\alpha_L)^3}\right] J_G^{*2-B'} + \left[\frac{2AN_L^{-B}}{\alpha_L^3}\right] J_L^{*2-B} \approx 1 \tag{38}$$

Differentiating this equation with respect to α_L and eliminating α_L from the resultant equation yield the following fundamental functional form of CCFL correlation:

$$\left(\frac{2A'}{N_G^{B'}}\right)^{1/4} J_G^{*1/2-B'/4} + \left(\frac{2A}{N_L^B}\right)^{1/4} J_L^{*1/2-B/4} \approx 1 \tag{39}$$

Since the Kutateladze parameter is more appropriate than the Wallis parameter when correlating flooding curves in large diameter pipes (Vijayan et al., 2001; Wynne et al., 2016) and CCFL characteristics of CCFL-U (Doi et al., 2012), Eq. (39) expressed in terms of Ku would be also useful:

$$\left(\frac{2A'Oh_G^{B'}}{D^{*B'/2}}\right)^{1/4} Ku_G^{*1/2-B'/4} + \left(\frac{2AOh_L^B}{D^{*B/2}}\right)^{1/4} Ku_L^{*1/2-B/4} \approx D^{*1/4} \tag{40}$$

where the gas Ohnesorge number is defined by

$$Oh_G = \sqrt{\frac{\mu_G^2}{\rho_G \sigma D}} \tag{41}$$

3.2. Reducing fundamental functional form to available correlations

Let us consider some limiting cases to deduce available CCFL correlations from the fundamental functional form. If the gas volume flux is large, the interface would be largely disturbed and the skin friction must be overcome by the form drag. Hence f_i may depend only on α_L, and therefore, $B' = 0$ in Eq. (39).

$$J_G^{*1/2} + \left(\frac{A}{A' N_L^B}\right)^{1/4} J_L^{*1/2-B/4} \approx (2A')^{-1/4} \tag{42}$$

If the viscous effect in f_W is neglected, i.e. $B = 0$, we obtain

$$J_G^{*1/2} + \left(\frac{A}{A'}\right)^{1/4} J_L^{*1/2} \approx (2A')^{-1/4} \tag{43}$$

which reduces to Eq. (1) by setting $m = (A/A')^{1/4}$ and $C = (2A')^{-1/4}$. If the liquid viscosity plays a role in CCFL, Wallis (1969) pointed out that m and C depend on N_L, and therefore, A' can be a function of N_L. Hence

$$J_G^{*1/2} + f'(N_L) J_L^{*1/2} \approx f''(N_L) \tag{44}$$

Assuming that the function, $f'(N_L)$, is given by $f'(N_L) = 5.6/N_L^{1/2}$ and $f'' = 0.725$ yields Eq. (4).

If the Taylor length $l_T = \sqrt{\sigma/\Delta\rho g}$ is comparable to D,

$$N_L \approx Oh_L^{-1} \tag{45}$$

Eq. (44) corresponds to the Zapke-Kröger correlation by setting $f' = 1$ and $f''(N_L) \approx f''(Oh_L^{-1}) = 0.52 Oh_L^{-0.05}$.

4. Application of derived functional form to CCFL

4.1. CCFL characteristics with sharp-edged lower end

The end shape of a vertical pipe is known to affect the location of flooding (Wallis, 1969). CCFL data must therefore be carefully selected for the same end shape when using them to determine the model constants in CCFL characteristics. However the CCFL location has rarely been reported in literature. In Kusunoki et al. (2015), they obtained the CCFL characteristics for CCFL at the sharp-edged lower end of a vertical pipe (CCFL-L). In this section the fundamental functional form is reduced to the CCFL characteristics correlation for CCFL-L by making use of the CCFL data given in Kusunoki et al. (2015).

Figure 2 shows the CCFL characteristics of four two-phase systems, i.e. air-water, steam-water, air-glycerol water solution of 40 wt%, and air-glycerol water solution of 60 wt%. The pipe diameter was 20 mm and the experiments were carried out at atmospheric pressure. The N_L ranged from 1.1×10^3 (60% glycerol-water solution) to 3.0×10^4 (steam-water). See Kusunoki et al. (2015) for more detail.

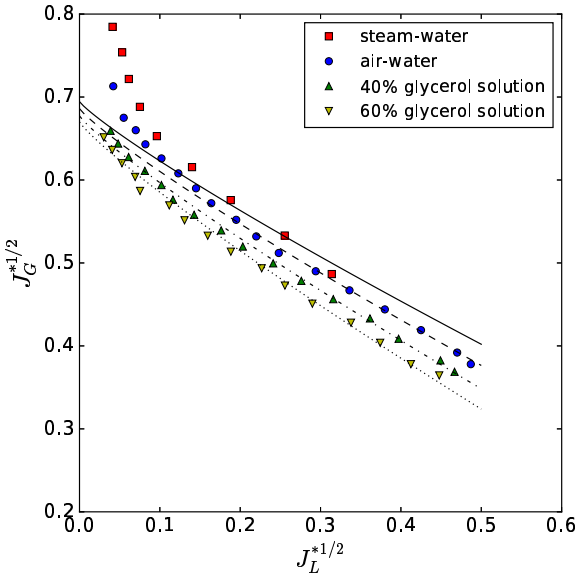

Figure 2: CCFL characteristics of CCFL-L in vertical pipe of $D = 20$ mm (Kusunoki et al., 2015). Lines are Eq. (49) (solid line: steam-water, dashed line: air-water, dash-dotted line: 40% glycerol solution, dotted line: 60% glycerol solution).

Since the gas flow was turbulent under all the experimental conditions, let us neglect the viscous effect in f_i, i.e. $B' = 0$. The fundamental functional form, Eq. (39), therefore reduces to

$$J_G^{*1/2} + \left(\frac{A}{A' N_L^B}\right)^{1/4} J_L^{*1/2-B/4} \approx \left(\frac{1}{2A'}\right)^{1/4} \tag{46}$$

According to the fact that m and C in Eq. (1) depend on N_L, we assume $A' = \Lambda N_L^V$, where Λ and V are constants. The CCFL characteristics are therefore given by

$$J_G^{*1/2} + \left(\frac{m_L}{N_L^{(B+V)/4}}\right) J_L^{*1/2-B/4} = \frac{C_L}{N_L^{V/4}} \tag{47}$$

where m_L and C_L are constants. The CCFL data, especially for the air-water and steam-water systems, show that the slopes change at about $J_L^{*1/2} = 0.1$. The Re_L increases with increasing $J_L^{*1/2}$ and, at large J_L, Re_L becomes larger than 150, which is the critical Re_L for laminar-turbulent liquid film transition (Aragaki et al., 1987). Hence let us apply $B = 1/4$ by assuming turbulent film flow:

$$J_G^{*1/2} + \left(\frac{m_L}{N_L^{(1+4V)/16}}\right) J_L^{*7/16} = \frac{C_L}{N_L^{V/4}} \tag{48}$$

Good evaluations of the CCFL characteristics at large $J_L^{*1/2}$ are obtained as shown in Fig. 2 by fitting the functional form to the data, i.e.

$$J_G^{*1/2} + \left(\frac{0.91}{N_L^{0.052}} \right) J_L^{*7/16} = 0.62 N_L^{0.011} \tag{49}$$

The correlation however largely deviates from the data of the steam-water and air-water systems at low $J_L^{*1/2}$, and therefore, the model parameters should be modified.

At low $J_L^{*1/2}$, J_G^* become extremely high and the gas-liquid interface of film flow will be highly disturbed, and therefore, let us assume $B = 0$:

$$J_G^{*1/2} + \left(\frac{m_L}{N_L^{V/4}} \right) J_L^{*1/2} = \frac{C_L}{N_L^{V/4}} \tag{50}$$

Fitting this functional form to the data gives

$$J_G^{*1/2} + 0.80 N_L^{0.051} J_L^{*1/2} = 0.474 N_L^{0.051} \tag{51}$$

The combination of Eqs. (49) and (51) gives good evaluations as shown in Fig. 3, where $J_G^{*1/2}$ was calculated using Eqs. (49) and (51), and then, the larger one was plotted at each $J_L^{*1/2}$. The errors are less than $\pm 10\%$ as shown in Fig. 4.

Bharathan and Wallis (1983) obtained the CCFL characteristics of the air-water system for $D = 51$ mm. Zapke and Kröger (1996) investigated the effects of the liquid viscosity and the surface tension on the CCFL characteristics by using several liquids and a vertical pipe of $D = 30$ mm. They used water, propanol, methanol and aqueous methanol solutions for the liquid phase. The ranges of ρ_L, μ_L and σ are as follows: $784 \leq \rho_L \leq 998$ kg/m^3, $1 \leq \mu_L < 2.3$ mPa·s, and $0.022 \leq \sigma \leq 0.072$ N/m. The flow limitation occurred at the sharp-edged lower ends of the vertical pipes in their experiments, i.e. CCFL-L. We shall make use of their data to examine the applicability of the present correlations, Eqs. (49) and (51), to the larger D and the various fluid properties.

Figure 5 shows comparisons between the combination of Eqs. (49) and (51) and the data. The correlation gives a good agreement with the Zapke-Kröger data. Though the errors for the Bharathan data are relatively larger, they lie to within $\pm 10\%$ errors. The comparisons confirmed that the present correlation is also applicable to the CCFL-L of larger D and various fluid properties.

The liquid lump had the primal contribution to the flow limitation in CCFL-L (Kusunoki et al., 2015). Its shape was largely agitated by the gas flow and drops flowed with the liquid lump. Other sources of flow limitation are also possible, e.g. droplets caused by entrainment inside the pipe. A possible improvement of the proposed model to account for such contributions to the flow limitation is to use multi-fluid equations. However there are no available models for the droplet entrainment and deposition under CCFL conditions, and therefore, the multi-fluid modeling of the CCFL characteristics is a challenging task to be pursued in the future.

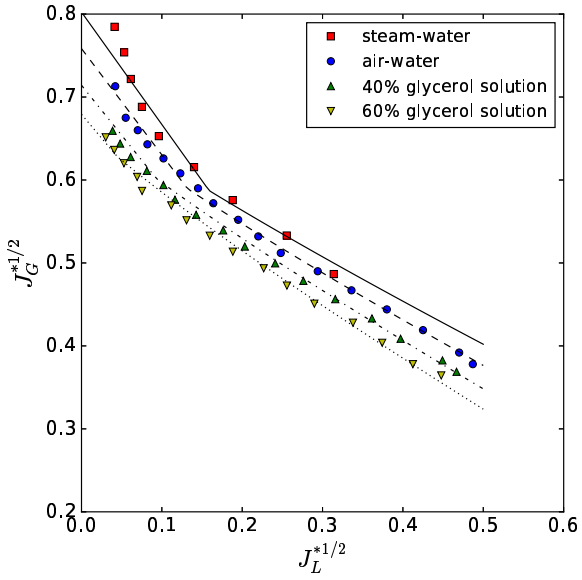

Figure 3: CCFL correlation, Eqs. (49) and (51), compared with CCFL-L data (Kusunoki et al., 2015). (solid line: steam-water, dashed line: air-water, dash-dotted line: 40% glycerol solution, dotted line: 60% glycerol solution)

4.2. CCFL characteristics with sharp-edged upper end

The derived fundamental functional form is adopted to the data of CCFL-U reported in Doi et al. (2012). Under CCFL-U, most of liquid penetration from the upper tank into the pipe takes place during bubble detachment at the junction between the tank and the pipe end. The balance between the buoyancy and the surface tension force in the bubble generation process might therefore play an important role in the CCFL characteristics. By neglecting the inertia effect, the balance can be evaluated by

$$\Delta\rho g D^3 = C_b^4 D\sigma \tag{52}$$

where C_b is a constant. Hence

$$\frac{D}{\sqrt{\frac{\sigma}{\Delta\rho g}}} = C_b^2 \tag{53}$$

Equivalently

$$D^{*1/2} = C_b \tag{54}$$

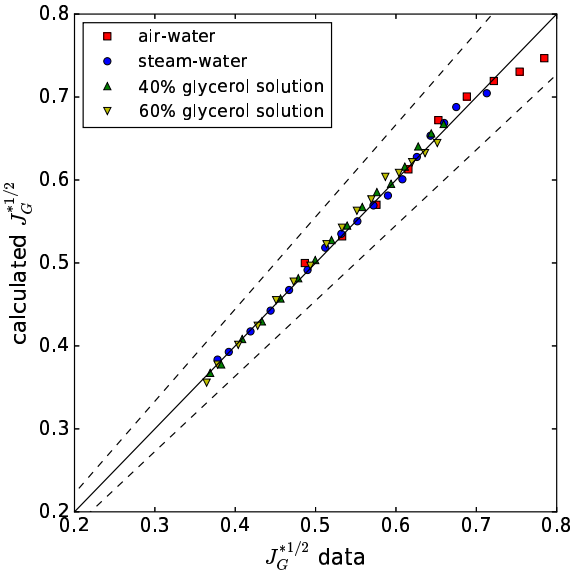

Figure 4: Comparisons between $J_G^{*1/2}$ calculated using CCFL characteristics correlation, Eqs. (49) and (51), and in CCFL data of Kusunoki et al. (2015) (dotted lines represent ±10% errors)

By using this approximation, the fundamental functional form in terms of Ku_k, Eq. (40), reduces to

$$(2A')^{1/4}\left(\frac{Oh_G}{C_b}\right)^{B'/4} Ku_G^{*1/2-B'/4} + (2A)^{1/4}\left(\frac{Oh_L}{C_b}\right)^{B/4} Ku_L^{*1/2-B/4} \approx C_b^{1/2} \tag{55}$$

The experimental fact that D has no influence on the CCFL characteristics of CCFL-U indicates $B = B' = 0$. Thus

$$Ku_G^{*1/2} + m_U Ku_L^{*1/2} \approx C_U \tag{56}$$

where

$$m_U = \left(\frac{A}{A'}\right)^{1/4} \tag{57}$$

$$C_U = \frac{C_b^{1/2}}{(2A')^{1/4}} \tag{58}$$

As carried out in Murase et al. (2016), fitting to the above functional form to the data gives $m_U = 0.90$ and $C_U = 1.5$. The correlation agrees with the data as reported in Murase et al. (2016), in which one can find detailed discussion on the CCFL-U correlation. The constants are related with the coefficients in the friction factors. The correlation would therefore be improved by obtaining databases of the friction factors under CCFL-U.

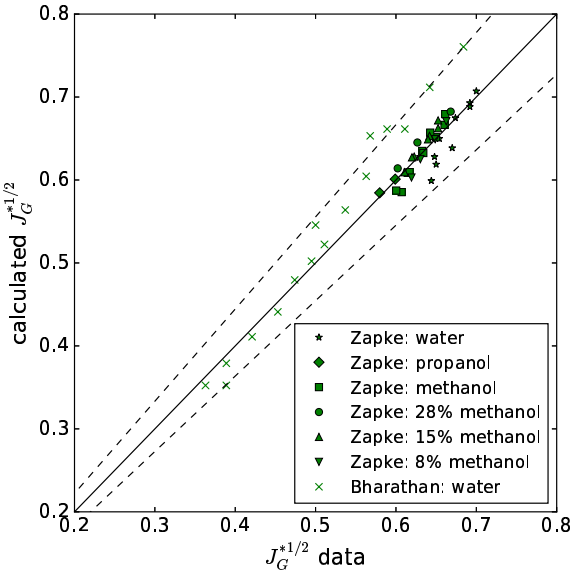

Figure 5: CCFL correlation compared with flooding data (Bharathan and Wallis, 1983; Zapke and Kröger, 1996) (dotted lines represent ±10% errors)

5. Conclusion

A semi-empirical correlation for counter-current flow limitation was derived from the one-dimensional momentum equations for counter-current annular two-phase flows in vertical pipes. The fundamental functional form of the CCFL correlation in terms of the Wallis parameters was obtained as an envelope of the momentum balance equation. The Kutateladze parameters can also be used in the functional form instead of the Wallis parameters. Limiting cases for the interfacial and wall friction factors show that the derived fundamental functional form reduces to available CCFL correlations. The model parameters in the fundamental functional form were determined for the data of CCFL at the sharp-edged lower end of a vertical pipe, so that the correlation gave good evaluations not only of the CCFL characteristics data used for fitting but also for other data in literature. By considering the bubble generation process at the junction between a vertical pipe and an upper tank connected to the pipe under CCFL at the upper end, the Kutateladze-type CCFL characteristics correlation was obtained. Thus the present fundamental functional form is of use not only to express CCFL data but also to understand how relevant parameters play their roles in the CCFL characteristics.

Acknowledgement

This work has been supported by JSPS KAKENHI Grant Number 15H03920.

References

Abe, Y., Akimoto, H., Murao, Y., 1991. Estimation of shear stress in countercurrent annular flow. Journal of Nuclear Science and Technology 28(3), 208–217.

Aragaki, T., Toyama, M., Salah, H.-M., Murase, K., Suzuki, M., 1987. Transitional zone in falling liquid film. Kagaku-Kogaku Ronbunshu 13(3), 373–375.

Bankoff, S. G., Lee, S. C., 1986. A critical review of the flooding literature. In: Hewitt, G. F., Delhaye, J. M., Zuber, N. (Eds.), Multiphase Science and Technology. Vol. 2. Ch. 2, pp. 95–180.

Bharathan, D., Wallis, G. B., 1983. Air-water countercurrent annular flow. Internation Journal of Multiphase Flow 9(4), 349–366.

Doi, T., Futatsugi, T., Murase, M., Hayashi, K., Hosokawa, S., Tomiyama, A., 2012. Countercurrent flow limitation at the junction between the surge line and the pressurizer of a pwr. Science and Technology of Nuclear Installations 2012, 1–10.

Govan, A. H., Hewitt, G. F., Richter, H. J., Scott, A., 1991. Flooding and churn flow in vertical pipes. International Journal of Multiphase Flow 17(1), 27–44.

Jeong, J. H., No, H. C., 1996. Experimental study of the effect of pipe length and pipe-end geometry on flooding. International Journal of Multiphase Flow 22(3), 499–514.

Karimi, G., Kawaji, M., 2000. Flooding in vertical counter-current annular flow. Nuclear Engineering and Design 200, 95–105.

Kusunoki, T., Murase, M., Fujii, Y., Nozue, T., Hayashi, K., Hosokawa, S., Tomiyama, A., 2015. Effects of fluid properties on ccfl characteristics at a vertical pipe lower end. Journal of Nuclear Science and Technology 52(6), 887–896.

Kusunoki, T., Nozue, T., Hayashi, K., Hosokawa, S., Tomiyama, A., Murase, M., 2016. Condensation experiments for counter-current flow limitation in an inverted U-tube. Journal of Nuclear Science and Technology 53(4), 486–495.

Kusunoki, T., Yamamoto, Y., Murase, M., Hayashi, K., Hosokawa, S., Tomiyama, A., 2017. The hanging film phenomenon in vertical annular two-phase flow. Japanese Journal of Multiphase Flow 31(1), 37–46.

Murase, M., Kusunoki, T., Mori, K., Tomiyama, A., 2016. Countercurrent flow limitation in vertical pipes with the sharp-edged upper end. In: Proceedings of the 11th International Topical Meeting on Nuclear Reactor Thermal Hydraulics, Operation and Safety. Gyeongju, Korea, pp. 1–10.

Richter, H. J., 1981. Flooding in tubes and annuli. International Journal of Multiphase Flow 7(6), 647–658.

Schmidt, P., Náraigh, L. Ó., Lucquiaud, M., Valluri, P., 2016. Linear and non-linear instability in vertical counter-current laminar gas-liquid flows. Physics of Fluids 28, 042102.

Vijayan, M., Jayanti, S., Balakrishnan, A. R., 2001. Effect of tube diameter on flooding. International Journal of Multiphase Flow 27, 797–816.

Wallis, G. B., 1969. One-dimensional two-phase flow, 1st Edition. McGraw-Hill.

Wallis, G. B., Makkenchery, S., 1974. The hanging film phenomenon in vertical annular two-phase flow. Journal of Fluids Engineering 96(3), 297–298.

Wynne, N., Garza, M., Vierow, K., Aumiller, D., Kyle, M., 2016. Air-water and steam-water onset of flooding data at variable pressure in a large diameter tube. In: Proceedings of the International Topical Meeting on Advanced Reactors Safety. New Orleans, LA, USA, pp. 1–14.

Zapke, A., Kröger, D. G., 1996. The influence of fluid properties and inlet geometry on flooding in vertical and inclined tubes. Internation Journal of Multiphase Flow 22(3), 461–472.

Zapke, A., Kröger, D. G., 2000a. Countercurrent gas-liquid flow in inclined and vertical ducts -I: Flow patterns, pressure drop characteristics and flooding. Internation Journal of Multiphase Flow 26, 1439–1455.

Zapke, A., Kröger, D. G., 2000b. Countercurrent gas-liquid flow in inclined and vertical ducts -II: The validity of the froude-ohnesorge number correlation for flooding. Internation Journal of Multiphase Flow 26, 1457–1468.